HHS Public Access

Author manuscript

J Mol Neurosci. Author manuscript; available in PMC 2023 March 01.

Published in final edited form as:

J Mol Neurosci. 2022 June ; 72(6): 1243–1258. doi:10.1007/s12031-022-02030-w.

Impact of Raptor and Rictor deletion on hippocampal pathology following status epilepticus

Christin M. Godale[1,3], **Emma V. Parkins**[2,3], **Christina Gross**[2,3,4], **Steve C. Danzer**[1,3,4,5]

[1.]Cincinnati Children's Hospital Medical Center, Department of Anesthesia, Cincinnati, OH, USA

[2.]Cincinnati Children's Hospital Medical Center, Division of Neurology, Cincinnati, OH, USA

[3.]University of Cincinnati, Neuroscience Graduate Program, Cincinnati, OH, USA

[4.]Department of Pediatrics, University of Cincinnati College of Medicine, Cincinnati, OH, USA

[5.]Department of Anesthesiology, University of Cincinnati College of Medicine, Cincinnati, OH, USA

Abstract

Neuronal hyperactivation of the mTOR signaling pathway may play a role in driving the pathological sequelae that follow status epilepticus. Animal studies using pharmacological tools provide support for this hypothesis, however, systemic inhibition of mTOR – a growth pathway active in every mammalian cell – limits conclusions on cell type specificity. To circumvent the limitations of pharmacological approaches, we developed a viral/genetic strategy to delete Raptor or Rictor, inhibiting mTORC1 or mTORC2, respectively, from excitatory hippocampal neurons after status epilepticus in mice. Raptor or Rictor was deleted from roughly 25% of hippocampal granule cells, with variable involvement of other hippocampal neurons, after pilocarpine status epilepticus. Status epilepticus induced the expected loss of hilar neurons, sprouting of granule cell mossy fiber axons and reduced c-Fos activation. Gene deletion did not prevent these changes, although Raptor loss reduced the density of c-Fos positive granule cells overall relative to Rictor groups. Findings demonstrate that mTOR signaling can be effectively modulated with this approach and further reveal that blocking mTOR signaling in a minority (25%) of granule cells is not sufficient to alter key measures of status epilepticus-induced pathology. The approach is suitable for producing higher deletion rates, and altering the timing of deletion, which may lead to different outcomes.

[*]*Corresponding author, contact information:* steve.danzer@cchmc.org, 3333 Burnet Ave., Dept. Anesthesia, ML2001, Cincinnati, OH 45229.

Author Contributions:

Christin Margaret Godale (CMG), Dr. Steve Craig Danzer (SCD), and Dr. Christina Gross (CG) contributed to the experimental design and manuscript preparation. Data collection and analysis were performed by CMG, Emma Victoria Parkins (EVP), and SCD. All authors read and approved the final manuscript.

Conflict of Interest:

The authors have no relevant financial or non-financial interests to disclose.

Ethics Approval:

Animal studies were approved by the Cincinnati Children's Hospital Institutional Animal Care and Use Committee and are in accord with NIH guidelines for the care and use of animals.

Informed Consent:

This study does not involve human subjects.

Keywords

mTOR; mTORC1; mTORC2; dentate granule cells; temporal lobe epilepsy; c-Fos

1 INTRODUCTION

The mechanistic target of rapamycin (mTOR) is a serine/threonine kinase involved in a highly conserved phosphatidylinositol-3-kinase-Akt signaling pathway. The mTOR signaling pathway is a key mediator of cell growth throughout the body. Mutations causing mTOR pathway hyperactivation increase cellular growth, and are frequently found in tumors (Sarbassov et al., 2005). In the nervous system, mutations in mTOR pathway genes produce so called “mTORopathies”, which are associated with cognitive dysfunction, autism and epilepsy (Nguyen & Bordey, 2021).

The strong link between mTOR pathway mutations and genetic epilepsies has raised interest in whether dysregulation of mTOR signaling might also be involved in acquired epilepsy. Acquired epilepsy can result from a range of neurological insults, such as birth injuries, head trauma and stroke. Acquired epilepsies are not typically associated with mutations in the mTOR pathway; however, enhanced mTOR pathway signaling is evident in almost all rodent acquired epilepsy models that have been examined, including systemic kainic acid (Macias et al., 2013), intrahippocampal kainic acid (Gericke et al., 2020), traumatic brain injury (Guo et al., 2013) and pilocarpine status epilepticus (SE) (Okamoto et al., 2010). Moreover, enhanced mTOR signaling has also been observed in human patients with temporal lobe epilepsy (Talos et al., 2018).

Research exploring whether enhanced mTOR signaling mediates acquired epileptogenesis has largely revolved around using the mTOR antagonist rapamycin and its analogues. Studies have produced mixed results, with robust anti-seizure and anti-epileptogenic effects in some models, and little to no effect in others (Citraro et al., 2016; Löscher, 2020; Theilmann et al., 2020). The ubiquitous expression of mTOR, however, creates a problem for interpreting the effects of systemically applied drugs. Rapamycin, for example, has robust immunosuppressive effects and inflammation is an important component of many epilepsies (Vezzani et al., 2019). Where and how the drug acts to produce any effects and the potential for multisystemic and even competing effects of the drug complicates these pharmacological studies.

mTOR antagonists may produce their beneficial effects by acting on hippocampal dentate granule cells (DGC). Granule cells are hypothesized to play a key role in the development of temporal lobe epilepsy (Heinemann et al., 1992; Krook-Magnuson et al., 2015). The neurons exhibit enhanced mTOR signaling after epileptogenic brain injury in several acquired epilepsy models and undergo changes in cellular structure. Notably, granule cells exhibit mTOR dependent sprouting of their mossy fiber axons in epilepsy models (Butler et al., 2015; Guo et al., 2013; Tang et al., 2012a; Yamawaki et al., 2015; Zeng et al., 2009) providing direct evidence of mTOR dependent changes in this cell type. Granule cells, therefore, are a promising target for cell type-specific inhibition of mTOR signaling in epilepsy.

For the present study, we developed a combined viral/transgenic strategy to inhibit mTOR signaling among excitatory neurons in a mouse model of acquired epilepsy. This gene deletion approach targeted the *R*egulatory-*A*ssociated *P*rotein of m*TOR* (Raptor) and *R*apamycin-*I*nsensitive *C*ompanion of m*TOR* (Rictor), which are required for signaling through the two arms of the mTOR pathway, mTORC1 and mTORC2, respectively (Kim et al., 2002; Sarbassov et al., 2004). Signaling through both arms of the pathway has been implicated in epileptogenesis in different model systems (Chen et al., 2016; Chen et al., 2019; Karalis and Bateup, 2021). Using this approach, we targeted gene deletions to excitatory hippocampal dentate granule cells.

2. METHODS

2.1 Animals

Animal procedures were conducted in accordance with the National Institutes of Health's Guide for the Care and Use of Laboratory Animals and Cincinnati Children's Hospital Medical Center Institutional Animal Care and Use Committee (IACUC) guidelines. All mice were maintained on a C57BL/6 background. Raptor$^{fl/fl}$ mice (B6.Cg-Rptor$^{tm1.1Dmsa}$/J, RRID: IMSR_JAX:013188; Peterson et al., 2011; Sengupta et al., 2010) were crossed to homozygous tdTomato reporter mice (B6.Cg-Gt(ROSA)26Sor$^{tm9(CAG-tdTomato)Hze}$/J, RRID: IMSR_JAX:007909; Madisen et al., 2010) to generate Raptor$^{fl/fl}$, tdTomato$^{+/-}$ mice. Rictor$^{fl/fl}$ mice (Ptprc^{b} Thy1^{a} Rictor$^{tm1.1Klg}$/SjmJ, RRID: IMSR_JAX:020649; Magee et al., 2012; Tang et al., 2012b) were crossed to homozygous tdTomato reporter mice to generate Rictor$^{fl/fl}$, tdTomato$^{+/-}$ mice. Raptor$^{fl/fl}$, tdTomato$^{+/-}$ mice contain a loxP-flanked stop sequence in front of exon 6 of the targeted *Rptor* (regulatory associated protein of mechanistic target of rapamycin, complex 1) gene. Similarly, Rictor$^{fl/fl}$, tdTomato$^{+/-}$ mice contain a loxP-flanked stop sequence in front of exon 11 of the targeted *Rictor* (rapamycin-insensitive companion of the mechanistic target of rapamycin, complex 2) gene. Mice were weaned at 3 weeks of age and same-sex littermates were housed together (2 – 4 mice per cage) in standard cages with normal chow, water *ad libitum,* and a 14/10 light/dark cycle.

2.2 Western blot studies

To confirm the efficacy of viral-mediated gene deletion, Raptor and Rictor KO mice were generated for western blot analyses. Mice were anesthetized with 4.0% isoflurane (0.5 L/min) in oxygen, transferred to a stereotaxic frame (Model 942, Kopf Instruments) and then maintained at 0.5 – 0.7% isoflurane throughout the procedure. Following effective anesthesia, the animal's head was secured in a stereotactic device with a nose cone to administer continuous isoflurane. The scalp was injected subcutaneously with one dose of 0.05 mL of 2.0% lidocaine prior to incision and a single anterior-posterior cut was made along the scalp to expose the surface of the skull. Four burr holes were drilled through the skull and animals were injected with AAV9.CamKII.eGFP (AAV Control; Titer: 1.2 x 10^{11} vg/mL; Cat# 105541-AAV9; RRID:Addgene_105541) or AAV9.CamKII.eGFP-Cre (KO; Titer: 1.2 x 10^{11} vg/mL; Cat# 105551-AAV9, RRID:Addgene_105551) in both dorsal (A/P: −2 mm, M/L: ±1.2 mm, D/V: −2.8 mm) and ventral (A/P: −3.2 mm, M/L: ±2.8 mm, D/V: −3.2 mm) dentate gyri. Animals were injected with 1000 nl of virus solution per site at a rate of 200 nL/min using a UMP3T-1 (World Precision Instruments) automated syringe

pump, a 5 μl Neuro Syringe (Hamilton Company), and Micro4 controller (World Precision Instruments). The needle was left in the hippocampus for an additional three minutes to avoid reflux along the needle track. Following infusion, bone wax was used to fill the drill holes, a thin layer of dental cement was applied over the skull and the entire incision was closed with surgical sutures and resealed with Gluture (Abbott Laboratories). Mice were swabbed with Neosporin around the incision to minimize risk of infection. Mice recovered from the surgery in approximately 20 minutes in a 32° incubator. Once awake, mice were given a single dose of carprofen (5 mg/kg, i.p.) for pain management. Western blot studies included six groups of adult mice, as follows: 1) Raptor AAV control (N= 7 [3 F, 4 M], $Raptor^{fl/fl}$; $tdTomato^{+/-}$ injected with AAV9.CamKII.eGFP); 2) Raptor naïve (N=6 [3 F, 3 M]; $Raptor^{fl/fl}$; $tdTomato^{+/-}$ mice that did not undergo surgery); 3) Raptor KO (N= 6 [0 F, 6 M], $Raptor^{fl/fl}$; $tdTomato^{+/-}$ injected with AAV9.CamKII.eGFP-Cre); 4) Rictor AAV control (N= 6 [0 F, 6 M], $Rictor^{fl/fl}$; $tdTomato^{+/-}$ injected with AAV9.CamKII.eGFP); 5) Rictor naïve (N=7 [4 F, 3 M], $Rictor^{fl/fl}$; $tdTomato^{+/-}$ mice that did not undergo surgery); 6) Rictor KO (N= 6 [2 F, 4 M], $Rictor^{fl/fl}$; $tdTomato^{+/-}$ injected with AAV9.CamKII.eGFP-Cre).

Eight to ten weeks after virus injection, animals were sacrificed with pentobarbital (100 mg/kg). Whole hippocampi were dissected and stored immediately at −80°C until processing. Prior to protein assay, the samples were lysed in PA lysis buffer (50 mM Tris [pH 7.4], 40 mM NaCl, 1 mM EDTA [pH 8], 50 mM NaF, 10 mM Na pyrophosphate, 10 mM Na beta-glycerol phosphate, 0.5% Triton X-100 with 1X protease inhibitor and 1X phosphostop). Protein concentration was determined using Bio-Rad Protein Assay Dye (Hercules, California, USA; Cat: 5000006). Samples were mixed with SDS sample buffer and 10 μg of protein was loaded in duplicate on SDS-PAGE gels, then transferred to PVDF Transfer Membrane (Millipore Sigma, Darmstadt, Germany). Membranes were blocked using 5% milk for 1 hour and incubated overnight at 4°C in rabbit anti-Raptor monoclonal (Cell Signaling Technology, Cat# 2280, RRID: AB_561245) or rabbit anti-Rictor polyclonal (Cell Signaling Technology, Cat# 2140, RRID: AB_2179961) antibodies diluted 1:2000 in 5% bovine serum albumin (Sigma, CAS# 9048-46-8) prepared in 1% Tween in PBS (filtered). Membranes were then washed in 1% Tween in PBS and incubated with rabbit IgG HRP Linked Whole Antibody using a 1:2000 dilution (Millipore Sigma, Cat# GENA934, RRID: AB_2722659). Signals were detected with enhanced chemiluminescence using Pierce ECL Blotting Substrate (Thermo Scientific, Carlsbad, CA, USA, Cat# 32106). Signal intensities of proteins were normalized to BIII-Tubulin (1:2000, BioLegend, Cat# 802001, RRID: AB_2564645) staining on the same blot. The average of the duplicates was counted as one data point. Protein-specific signals on western blots were quantified densitometrically using NIH ImageJ software (Version 1.53j, RRID: SCR_001935) by an experimenter blind to study conditions.

2.3 Raptor and Rictor deletion after status epilepticus

To induce status epilepticus, 9–13-week-old male and female mice were treated with pilocarpine. Animal details are provided in Table 1. For SE induction, all mice received a subcutaneous (s.c.) injection of scopolamine methyl nitrate (1mg/kg; TCI America, Wellesley, MA; Cat# S0230), followed 30 minutes later by 360-400 mg/kg pilocarpine (Sigma, St. Louis, MO; Cat# P6503) or saline. Mice treated with pilocarpine were monitored

for behavioral seizures and the onset of SE (Hester & Danzer, 2013). Three hours after the onset of SE, pilocarpine and control mice received two injections of diazepam (10 mg/kg) at 15 minutes intervals. Pretreatment body weight was maintained using sterile Ringer's solution s.c. to avoid potential SE-related dehydration. Only mice that experienced at least one class V (tonic/clonic) seizure (Racine, 1972) and exhibited continuous seizure-like behavior during the three hour observation period were included in the study (Hester et al., 2016). Following SE, mice were housed in a 32°C incubator overnight. The next morning, mice were weighed, given warm Ringer's solution (1-2 mL) s.c. to their pre-pilocarpine weight, and diet gel (ClearH2O, Westbrook, ME; Cat# 72074022). In the evening, the mice were re-weighed and given warmed Ringer's solution or returned to the incubators as needed. On the following day, mice were weighed in the morning and evening, given warmed Ringer's solution as needed, and returned to their normal housing environment with food and water *ad libitum*.

Four to eleven days after status epilepticus, animals were infused with a cocktail of AAV9.CamKII.eGFP (Titer: 4 x 10^9 vg/mL; Cat# 105541-AAV9; RRID:Addgene_105541) and AAV9.CamKII.Cre (Titer: 4 x 10^9 vg/mL; Cat# 105558-AAV9, RRID:Addgene_105558) targeting the dorsal dentate gyrus (2 injections/mouse; A/P: −2 mm, M/L: ± 1.2 mm, D/V: −2.8 mm) or the dorsal and ventral dentate gyrus (4 injections/mouse; A/P: −3.2 mm, M/L: ±2.8 mm, D/V: −3.2 mm). Saline-treated (No-SE) mice received identical infusions 7-14 days after saline treatment. Animals were injected with 500-1000 nL of the cocktail per site as described for western blot studies. AAV9.CamKII.eGFP was injected as part of another study. This AAV construct is a GFP expression vector targeting excitatory neurons. It was given to all animals and is not expected to impact the results of the present study.

2.4 Tissue processing and immunohistochemistry

Seven to ten weeks after virus injection, mice were anesthetized with pentobarbital (100 mg/kg) and transcardially perfused with heparinized PBS (1 U/mL) followed by 2.5% paraformaldehyde (PFA) with 4.0% sucrose in PBS chilled on ice. Harvested brains were dissected and fixed overnight in 2.5% PFA with 4.0% sucrose in PBS at 4°C. Brains were cryoprotected with sucrose (10%, 20%, and 30%) in PBS at 4°C for a minimum of 24 hours per step. Cryoprotected brains were snap-frozen in 4-methyl butane chilled to −25°C and stored at −80°C until further use. Brains were sectioned coronally at a thickness of 40 μm using a cryostat cooled to −22°C and mounted onto gel-coated glass slides. Sections were mounted 3 per slide in a 1 in 18 series such that each slide contained tissue from the dorsal-ventral extent of the hippocampus. Sections were left to dry at room temperature for two hours and then stored at −80°C until used for immunohistochemistry. The following histological and immunohistochemical procedures were conducted to characterize hippocampal morphology: 1) Neurotrace™ 640/660 deep-red Nissl staining (ThermoFisher, Waltham, MA; Cat# N21483) was used to characterize hilar cell loss; 2) rabbit anti-phospho-240/244-S6 diluted at 1:500 (pS6 antibody, Cat# 9468 RRID: AB_2716873) immunostaining was used to assess activation of the mTOR pathway; 3) rabbit anti-c-Fos diluted at 1:1000 (c-Fos antibody, Cat# ab222699, RRID: AB_2891049) immunostaining was used to assess immediate early gene activation throughout the dentate

granule cell layer; 4) rabbit anti-zinc transporter 3 diluted at 1:3000 (ZnT-3 antibody, Cat# 197 003DY5, RRID: AB_2737038) immunostaining was used to assess mossy fiber sprouting in the inner molecular layer (IML). For immunostaining, tissue sections mounted onto gelatin-coated slides were placed in blocking solution (4% normal goat serum, 0.1% bovine serum albumin, and 0.2% Triton-X in 0.1 M PBS) for 1 hour and subsequently incubated in rabbit anti-pS6, rabbit anti-cFos, or rabbit anti-ZnT-3 for 24h at 4°C. Goat-anti rabbit AlexaFluor 647 antibodies diluted at 1:750 (AlexaFluor 647, Cat# A32733TR, RRID: AB_2866492) were used to visualize the respective primary antibodies. Stained tissue sections were coverslipped with ProLong™ Glass Antifade Mountant with NucBlue™ (Thermofisher Scientific, Waltham, MA, Cat# P36981) mounting media. All analyses and counts were conducted by an investigator unaware of treatment group.

2.5 Quantification of viral spread in each animal

Viral spread was assessed from three brain sections (6 dentate gyri) per animal from a 1 in 18 coronal series through the hippocampus. tdTomato expression, indicative of cre recombinase activity, was used as a proxy marker for viral infection of the dentate gyrus. Expression was scored using a semiquantitative 0-4 scale ranging from 0 (0%), 1 (<25%), 2 (25-50%), 3 (50-75%), and 4 (>75%) of dentate granule cells expressing the tdTomato reporter. Scoring was conducted by an investigator blind to treatment group using a Leica DMI6000 CS inverted microscope under 10X magnification. Scores reflect estimates of the percentage of granule cells in the section regardless of whether labeling was dispersed through the upper and lower blades or concentrated in a portion of the dentate. Viral expression was also evident in CA1 pyramidal cells, CA3 pyramidal cells, cortical excitatory cells, and thalamic neurons. To characterize this expression, six brain sections per animals from the 1 in 18 coronal series were scored by an investigator blind to group using a Nikon AXR Inverted microscope under 10X magnification. Animals were scored as having expression in a region if one or more brain sections contained tdTomato labeled cells. Animal scores (expression present/not present) were compiled to generate the percentage of animals in each study group that had some expression in the four regions.

2.6 Quantification of hilar cell loss and hilar volume

Loss of neurons in the dentate hilus was quantified from two 40 μm brain sections per mouse (Bregma = −1.58 to −2.4) stained with Neurotrace™ 640/660. Sections were imaged with a Nikon AIR LUN-V Inverted Microscope (20x objective, NA=0.75, resolution = 0.62 μm/pixel, 1 μm step through the z-axis). Confocal z-stacks were imported into Nikon Elements software (Version 5.2.1, RRID: SCR_014329) for quantification. The hilus was defined by the hilar-granule cell body layer border, with the lateral extent defined by a line connecting the tips of the upper and lower blades of the granule cell body layer. Within the hilus, all labeled cells with diameters exceeding 20 μm were counted using a modified stereological approach (Hofacer et al., 2013). The size restriction was included to exclude smaller non-neuronal cells and ectopic granule cells from the count. Hilar cell density was calculated by dividing cell counts by hilar volume examined.

2.7 Quantification of c-Fos expression

To determine whether Raptor or Rictor deletion impacts neuronal activity in the home cage environment, brain sections were immunostained for c-Fos. Immunoreactivity for c-Fos was imaged from two dentate gyri per animal (Bregma = −1.58 to −2.4) using a Nikon AIR LUN-V Inverted Microscope (Objective = 20x, NA=0.75, resolution = 0.63 μm/pixel, z-step = 0.5-1 μm). Confocal z-stacks were imported into Neurolucida 360 software (Version 2021.1.3, RRID: SCR_016788) for quantification. An investigator blind to treatment group identified c-Fos immunoreactive cells in the dentate granule cell body layer, excluding the molecular layer and hilus. Results were obtained with Neurolucida Explorer (Version 2021.1.1, RRID: SCR_017348) and are reported as density measurements (total c-Fos+ cells/DGC-L volume).

2.8 Mossy fiber sprouting analysis

Brain sections immunostained with zinc transporter 3 (ZnT-3) were screened to identify mossy fiber sprouting, evident as ZnT-3 immunoreactive puncta in the dentate IML. ZnT-3 immunostained sections were imaged using Nikon AIR LUN-V Inverted Microscope (Objective = 60x, NA=1.27, resolution = 0.29 μm/pixel, z-step = 0.2 μm). Images from the upper and lower blades of two dentate gyri per animal (Bregma = −1.58 to −2.4) were assigned a score from 0-4 relative to the quantity of Znt3 immunoreactive puncta in the IML. Briefly, sections with no puncta were given a score of 0. Sections that had rare, scattered ZnT-3 immunoreactive puncta (<10) in the IML were given a score of 1. Sections with frequent but scattered puncta through the IML received a score of 2, while sections with intermittent dense puncta received a score of 3. Sections with a continuous dense band of ZnT-3 immunopositive puncta in the IML were assigned a score of 4. The investigator evaluating the ZnT-3 score for each animal was blind to the treatment group.

2.9 Statistics and Figure Preparation

All statistical analysis was conducted using GraphPad Prism (Version 9.3.1, RRID: SCR_002798) or Sigma Plot (Version 14.5, RRID: SCR_003210). Two-Way ANOVA with genotype and treatment (SE/no SE) as factors was used to analyze AAV spread, hilar cell damage, c-Fos density, and ZnT-3 scores. Significance was defined as a p-value ≤0.05. Data that failed tests of normality or equal variance were ranked for analysis. For c-Fos density data, outliers were identified using the ROUT method in GraphPad Prism with Q=5%. All graphs were prepared in GraphPad Prism software. Values presented in graphs are ± standard error of the mean (SEM). Each data point in the graphs represents averaged scores from an individual animal.

All images are confocal maximum projections exported as TIFF files from Nikon Elements (Version 5.2.1, RRID: SCR_014329) and imported into Adobe Photoshop (Version 2022, RRID: SCR_014199). Color, brightness, and contrast were adjusted to enhance image details. Identical adjustments were made to all images meant for comparison

3 RESULTS

3.1 Deletion of Raptor and Rictor from excitatory hippocampal neurons

To delete Raptor or Rictor for western blot analyses, Raptor$^{fl/fl}$, tdTomato$^{+/-}$ and Rictor$^{fl/fl}$, tdTomato$^{+/-}$ mice received hippocampal injections of an adeno-associated virus containing a cre-recombinase gene driven by the CamKII promoter (Fig. 1a–b; KO, AAV9.CamKII.eGFP-Cre). The CamKII promotor restricts cre-recombinase expression to excitatory neurons, leading to selective loss of Raptor or Rictor from this population. Control animals received an eGFP expression vector (AAV9.CamKII.eGFP) or no treatment (naïve). For western blot analyses, animals received high-titer virus injections to infect large numbers of hippocampal principal cells. Lower titer injections were used to target the dentate gyrus more selectively in subsequent experiments, however, this smaller deletion was found to be suboptimal for detecting protein reductions in western blot, where the effect is diluted by non-infected cells in the homogenates (data not shown).

Western blot analyses of hippocampal homogenates from Raptor KOs (Fig. 1c,e; n=6) confirmed significant reductions in Raptor protein levels relative to naïve mice (n=6; one-way ANOVA with post-hoc Tukey test, p=0.0136) and Raptor AAV Controls (n=7; one-way ANOVA with post-hoc Tukey test, p=0.0024). Similar results were obtained with Rictor$^{fl/fl}$, tdTomato$^{+/-}$ mice (Fig. 1d,f), with Rictor KOs (n=6) having significantly lower Rictor protein levels than naïve mice (n=7; one-way ANOVA with post-hoc Tukey test, p=0.0008) and Rictor AAV Controls (n=6; p=0.0013). These results indicate that the model system is working as expected to delete Raptor or Rictor.

3.2 Deletion of Raptor and Rictor following status epilepticus

Activation of the mTOR signaling pathway is hypothesized to contribute to pathological brain changes following SE. The hippocampal dentate gyrus undergoes extensive changes after SE and may be a primary target for mTOR action. To examine the impact of mTOR signaling on the development of post-SE histopathology, we used the strategy developed here to delete Raptor or Rictor from dentate granule cells after SE. SE was induced with pilocarpine in adult Raptor$^{fl/fl}$, tdTomato+/− and Rictor$^{fl/fl}$, tdTomato+/− mice (Table 1), followed by AAV9.CamKII.Cre injection into the dentate gyrus (Fig. 2a).

We first confirmed effective stereotaxic targeting of the dentate in all animals by examining expression of the cre-dependent reporter tdTomato. Tomato expression among granule cells was scored in all animals using a semi-quantitative 0-4 scale for the percentage of infected granule cells (Fig. 2b; 0 [0%], 1 [<25%], 2 [25-50%], 3 [50-75%], and 4 [>75]) Mean scores for No-SE, Raptor KO (1.05±0.27), SE+Raptor KO (1.46±0.28), No-SE, Rictor KO (1.20±0.26), SE+Rictor KO (1.41±0.44), No-SE, wildtype (1.62±0.28), and SE wildtype (1.56±0.30) mice were statistically identical (p=0.7549; Two-Way ANOVA), confirming that expression patterns were similar across all study groups (Fig. 2c). Values roughly correspond to the deletion of Raptor or Rictor from 25% of granule cells in the KO animals, however, it is important to note that this deletion rate is the average across the entire dorsal-ventral extent of the hippocampus. Infection rates often exceeded 75% near the injection site, tapering off to near 0% distally. In addition to infection rates, efficacy at targeting the

dentate was also reviewed. AAV9 can be picked up by axons (Castle et al., 2014) and diffusion of virus away from the injection site will expand the target region. In addition to dentate granule cells, viral expression was evident in CA3, CA1, thalamus, and rarely the cortex. As expression in other cell types could impact study results, the percentage of animals with expression in each region is shown in Table 2.

mTOR signaling can regulate cell survival, so we queried whether KO cells appeared healthy. TdTomato-labeled Raptor and Rictor KO granule cells were grossly normal compared to labeled cells in wildtype animals, without obvious degenerative changes (Fig. 3). There was no statistical difference in percentages of labeled dentate granule cells among groups (Fig. 2), supporting the conclusion that deletion of Raptor or Rictor does not induce cell loss, as fluorescently labeled dying cells become pyknotic and are cleared from the brain quickly (hours to days) (Jiang et al., 2016).

3.3 Activation of downstream signaling among KO cells

Although western blot analyses were not suitable for confirming the efficacy of the smaller dentate deletions, we were able to take advantage of immunohistochemical reagents for detecting one of the downstream targets of Raptor/mTORC1: phosphorylated S6 (pS6). Immunostaining for pS6 in Raptor KO animals revealed loss of immunostaining in tdTomato-expressing regions of the dentate and a paucity of tdTomato positive, pS6 immunoreactive cells (Fig. 4b) relative to tissue from control (Fig. 4a) animals. No loss of pS6 immunolabeling was evident in Rictor KO tissue (Fig. 4c), the latter being consistent with the distinct targets of the Rictor/mTORC2 arm. Unfortunately, antibodies for Rictor protein and mTORC2 specific targets, such as phosphoAkt, were not found to be specific in our hands (data not shown). Nonetheless, the findings with Raptor KO/pS6 provide additional evidence that the deletion strategy is working as expected.

3.4 Hilar volume is increased and cell density is reduced after SE

Significant numbers of neurons, primarily excitatory mossy cells and interneurons, are lost in the dentate hilus in the days following SE (Wulsin et al., 2016). Although it is likely that most of these neurons were already dead before virus was infused to delete Raptor or Rictor, the intervention has the potential to alter subsequent cell loss. Consistent with prior studies, hilar cell density was significantly reduced in mice that underwent SE relative to animals that did not experience SE (Fig. 5b; Two-way ANOVA with treatment [SE/no SE] and genotype as factors, main effect of treatment, $p<0.001$). Cell density was significantly reduced by SE within all three genotypes (Holm-Sidak; $p<0.001$). No effect of genotype on hilar cell density was found ($p=0.116$) and there was no interaction between factors ($p=0.340$).

In addition to hilar neuron loss, the volume of the hilus increases after SE (Wulsin et al., 2021). Reductions in cell density, therefore, reflect a combination of cell loss and increased hilar volume. We queried, therefore, whether Raptor or Rictor deletion altered hilar volume. Hilar volume was significantly increased in mice that underwent SE relative to no SE controls (Fig. 5c; Two-way ANOVA with treatment [SE/no SE] and genotype as factors, main effect of treatment on ranked data, $p<0.001$). Volume was significantly increased by

SE within wildtype (Holm-Sidak; $p<0.001$) and Raptor KOs ($p=0.011$) and showed a trend in Rictor KOs ($p=0.097$). No effect of genotype on hilar volume was found (Two-way ANOVA; $p=0.699$) and there was no interaction between factors ($p=0.397$).

3.5 Mossy fiber sprouting in Raptor and Rictor KOs

Sprouting of granule cell mossy fiber axons into the dentate inner molecular layer (IML) is a characteristic feature of temporal lobe epilepsy in both animal models and humans (Godale & Danzer, 2018; Koyama and Ikegaya, 2018). We queried, therefore, whether Raptor or Rictor deletion would alter mossy fiber sprouting intensity. Mossy fiber sprouting was significantly increased in animals that underwent SE relative to no SE groups (Fig. 6; Two-way ANOVA with treatment [SE/no SE] and genotype as factors, main effect of treatment, $p<0.001$). Sprouting was significantly increased by SE within each genotype (Holm-Sidak; wildtype, $p<0.001$; Raptor, $p=0.008$; Rictor, $p=0.030$). No effect of either Raptor or Rictor deletion, however, was found on the degree of mossy fiber sprouting among groups (Two-way ANOVA; $p=0.439$). In addition, there was not a significant interaction between factors ($p=0.307$).

3.6 Impact of Raptor and Rictor deletion on c-Fos immunoreactivity

Finally, we examined the impact of SE and Raptor/Rictor deletion on the density of hippocampal granule cells immunopositive for the immediate early gene c-Fos. Immediate early gene expression can provide an indirect measure of neuronal activity. Although recent seizures dramatically increase c-Fos expression, epileptic animals typically spend much more time in interictal periods, when c-Fos activation can be lower than controls (Peng & Houser, 2005).

Gross examination of c-Fos immunoreactivity in the dentate granule cell body layer revealed relative consistency among animals that did not undergo SE, while SE wildtype and SE+Raptor KO groups were highly variable, including one animal in the former and two in the latter where large percentages of all granule cells were c-Fos immunoreactive, while other animals had very low expression (Fig. 7b). Perhaps due to this variability, statistical analyses revealed no effect of treatment ($p=0.209$) or genotype ($p=0.459$), and no interaction was found ($p=0.181$; Two-way ANOVA with treatment [SE/no SE] and genotype as factors on ranked data).

The three animals with high levels of c-Fos immunoreactivity likely experienced seizures in the hours prior to sacrifice, and all met criteria for exclusion as outliers (ROUT method). When these three animals were excluded from the data set, main effects of treatment ($p=0.020$) and genotype were found ($p=0.024$), but there was not a significant interaction between factors (Fig. 7c; $p=0.167$; Two-way ANOVA with treatment [SE/no SE] and genotype as factors on ranked data, main effect of treatment). The density of c-Fos immunoreactive cells was significantly reduced by SE within wildtype animals ($p=0.007$, Holm-Sidak), but not within Raptor or Rictor KOs. In addition, the density of c-Fos immunoreactive cells was significantly lower in Raptor KOs relative to Rictor KOs ($p=0.025$) but not to wildtype animals ($p=0.420$, Holm-Sidak).

4. DISCUSSION

For the present study, we queried whether deletion of the mTORC1 obligate adaptor protein Raptor, or the mTORC2 obligate adaptor protein Rictor, would alter pathological sequalae in the hippocampus following pilocarpine-induced SE. Readouts focused on four key pathologies that have consistently been found to be altered after SE: 1) Hilar cell loss; 2) Increased hilar volume; 3) Mossy fiber sprouting and 4) Reduced c-Fos labeling. All four readouts showed the predicted changes in wildtype animals that underwent status epilepticus. Neither Raptor nor Rictor deletion altered the first three measures, while a modest effect of Raptor deletion on c-Fos labeling was observed. Findings suggest that deletion of Raptor or Rictor from approximately 25% of the granule cell population beginning 1-2 weeks after SE is not sufficient to substantially alter the histopathological changes induced by status epilepticus.

mTOR signaling in acquired epilepsy

A key goal of the present study was to develop genetic strategies to facilitate cell-specific inhibition of mTOR pathway signaling in an acquired epilepsy model. Pharmacological approaches to inhibit mTOR signaling have shown promising anti-seizure effects in some epilepsy models, but have had little effect in others (Löscher, 2020). Multiple mechanisms likely contribute to epileptogenic brain injury, and these mechanisms likely vary among models. It is perhaps not unsurprising, therefore, that mTOR antagonists might show efficacy in some models but not others. The conflicting findings highlight a key challenge of pharmacological studies, in that deciphering exactly where a drug acts to produce an effect is not certain. This is especially true for mTOR antagonists, as the pathway is active in all mammalian cells, and is a key regulator of multiple systems implicated in epilepsy. One might reasonably assume, for example, that mTOR antagonists such as rapamycin produce brain specific effects by acting on the brain. The mTOR signaling pathway, however, is a critical regulator of both immune function and cellular metabolism. Systemic mTOR antagonism, therefore, might modulate injury from SE by reducing inflammation or altering metabolism either in the brain or periphery.

In addition to acting through diverse cellular targets, mTOR signaling in different cell types has the potential to exert opposing effects on pathological readouts. Among excitatory neurons, for example, studies consistently suggest that excess mTOR signaling is pathological. Genetic mutations that enhance mTOR signaling among excitatory neurons induce many of the pathologies examined here, including hilar neuron loss and granule cell mossy fiber sprouting (LaSarge et al., 2021; Pun et al., 2012). Conversely, mTOR activation among other cell types may be protective. Specifically, in the pilocarpine model, systemic mTOR inhibition with rapamycin blocked interneuron sprouting (Buckmaster & Wen, 2011), a potentially compensatory change in the context of epilepsy. Similarly, microglial specific deletion of mTOR worsened neuronal loss and increased seizure incidence in the pilocarpine model of epilepsy (Zhao et al., 2020). Studies assessing the tissue and cell type specific effects of mTOR signaling, therefore, are needed to decipher the mechanisms by which the pathway modulates brain injury. The techniques outlined here expand the toolkit for conducting these types of studies.

Reduced c-Fos in Raptor KOs

c-Fos protein can be produced within minutes of neuronal depolarization, and is commonly used as a marker of neuronal activity levels. Protein levels are dramatically increased in the minutes and hours after seizures, but then drop below baseline control levels during interictal periods (Peng & Houser, 2005). In the pilocarpine model, the density of c-Fos immunoreactive cells is chronically reduced in many brain regions, including the dentate (Wulsin et al., 2021). Within wildtype animals, a corresponding effect was observed in the present study. Raptor and Rictor KOs, on the other hand, exhibited relatively equal densities between saline and SE groups. The apparent absence of a reduction in c-Fos+ cell density in the KOs is intriguing, but should be interpreted cautiously, as a significant interaction between genotype and response to SE was not observed. The overall reduced density of c-Fos+ cells in Raptor KOs relative to Rictor KOs, however, was significant, and suggests that Raptor loss decreases baseline activity levels in the dentate gyrus while Rictor loss does not. Findings are consistent with studies showing that Raptor loss decreases excitatory synaptic transmission. Interestingly, both Raptor and Rictor loss can reduce synaptic transmission, but while Raptor appears to act through a postsynaptic mechanism, Rictor has been shown to act presynaptically (McCabe et al., 2020). Correspondingly, the mTORC1 antagonist rapamycin can reduce the number of AMPA receptors and prevent increases in spine density and mEPSC amplitude (Hernandez et al., 2012; Tang et al., 2002; Wang et al., 2006; Weston et al., 2012; Williams et al., 2015; Xiong et al., 2012). Rictor/Mtorc2, on the other hand, phosphorylates multiple PKC isoforms (i.e., PKCα, PKCβ, PKCγ, and PKCε). These PKC isoforms are implicated in regulating neurotransmitter release (Chu et al., 2014; Fujita et al., 1996). Reduced c-Fos in Raptor KO DGCs relative to Rictor KOs, therefore, might reflect postsynaptic actions of Raptor, which would impact DGCs directly, relative to effects on granule cell synapses, which might have a larger impact on their downstream targets.

Significance of the current findings

Several variables should be considered when interpreting the present study. Firstly, Raptor and Rictor deletion was initiated one-two weeks after SE. Because SE is not predictable in patient populations, treatments beginning after the insult have greater clinical relevance over pre-SE treatments. Treatments initiated before SE also run the risk of altering SE severity, a potentially significant confounding variable. Despite these advantages, however, delayed treatment comes with tradeoffs. Notably, many irreversible changes already occurred prior to gene deletion in our study. Substantial loss of hilar neurons, for example, is evident 48 hours after SE (Danzer et al., 2010). In addition, the viral strategy used here likely incurs some additional delays in the reduction of target proteins, as multiple steps occur between virus infection of the cell and cre-mediated deletion of the target gene. Even after gene deletion, residual protein may persist for some time, depending on protein turnover rates. While we have demonstrated that Raptor and Rictor protein levels are reduced at 8-10 weeks, preliminary findings with Raptor suggest the protein is still present at normal levels two weeks after viral infection (data not shown). Development of new strategies to delete Raptor more quickly after SE will be needed to establish whether earlier reduction of protein levels impacts SE pathology differently. A second key variable involves the size of the deletion. Viral titers were reduced to achieve more specific targeting of dentate granule cells given the hypothesized role of this structure as a key mediator of epileptogenesis.

Optimization, however, reduced overall expression to about 25% of the dentate on average (but variability was high and infection of other cell types was still observed). Larger deletion sizes and/or targeting a broader population of hippocampal neurons might produce greater effects. Notably, however, Krook-Magnuson and colleagues showed that small volumes of granule cells can be inhibited ontogenetically to prevent seizures (Krook-Magnuson et al., 2013); therefore, there is precedent to hypothesize that a 25% Raptor or Rictor deletion rate would be impactful. A third variable involves the use of the CamKII promoter. While effective, the CamkII promoter can drive gene deletion among other excitatory cells, which was noted here. These other cell types could account for the observed effects. Use of granule cell specific promotors in future studies will provide better information on the role of dentate granule cells. Restricting cre expression to mature excitatory neurons, which begins when neurons are around 4 weeks old with the CamkII promotor, could also be important (Arruda-Carvalho et al., 2014; Wang et al., 2013). In the pilocarpine model of epilepsy, two key pathological changes not examined here, specifically accumulation of ectopic granule cells, and *de novo* formation of granule cells with hilar projecting basal dendrites, occur among newly generated granule cells (Kron et al., 2010; Walter et al., 2007). Because the CamKII promotor only becomes active in mature neurons, gene deletion in the present study is predicted to occur after these pathologies develop. Aberrant activity among these newly generated neurons could contribute to readouts examined here among older cells. The opportune cell age to target gene deletions, however, remains an open question. While early gene deletion might produce greater reductions in pathology, disrupted mTOR signaling might also impair the differentiation or survival of newborn cells (Carson et al., 2012; Cloetta et al., 2013; Thomanetz et al., 2013; Ka et al., 2017; Malik et al., 2019). Finally, the study did not include seizure monitoring as a readout, as it was deemed more advantageous to focus on robust histological measures for this initial work utilizing this new model system. The present study should be interpreted with the noted caveats in mind. Future studies altering deletion timing and size may produce different results.

Conclusions

Here, we developed an approach to inhibit signaling through the two arms of the mTOR pathway, mTORC1 and mTORC2, among hippocampal granule cells to assess the role of these neurons in producing hippocampal pathologies following status epilepticus. The combination of AAV-mediated expression of cre-recombinase with transgenic lines containing floxed alleles of Raptor (blocking mTORC1), Rictor (blocking mTORC2) and a tdTomato reporter was effective under control conditions and following pilocarpine status epilepticus. The approach is easily modifiable to adjust deletion timing, size, and cellular targets (with different promoters) to continue to explore cell-type specific roles of mTOR signaling in brain pathology.

ACKNOWLEDGEMENTS

We would like to thank the Cincinnati Children’s Hospital Medical Center (CCHMC) Confocal Imaging Core for their assistance with confocal image acquisition and the CCHMC Division of Veterinary Services.

Funding:

This work was supported by the National Institute of Neurological Disorders and Stroke (SCD, R01-NS-062806, R01-NS-121042; CMG, F31-NS11552501), and the American Epilepsy Society (CMG, 2019 Predoctoral Fellowship).

ABBREVIATIONS

AAV	Adeno-associated virus
DGC	Dentate granule cell
DGC-L	Dentate granule cell body layer
IML	Inner molecular layer
mTOR	Mechanistic target of rapamycin
mTORC1	Mechanistic target of rapamycin complex 1
mTORC2	Mechanistic target of rapamycin complex 2
pS6	Phosphorylated S6
Raptor	Regulatory-associated protein of mTOR
Rictor	Rapamycin-insensitive companion of mTOR
SE	Status epilepticus
Vg	Viral genomes
ZnT-3	Zinc transporter 3

REFERENCES

Arruda-Carvalho M, Restivo L, Guskjolen A, Epp JR, Elgersma Y, Josselyn SA, Frankland PW (2014) Conditional deletion of α-CamKII impairs integration of adult-generated granule cells into dentate gyrus circuits and hippocampus-dependent learning. The Journal of Neuroscience, 34(36), 11919–11928. 10.1523/jneurosci.0652-14.2014 [PubMed: 25186740]

Buckmaster PS, Wen X (2011) Rapamycin suppresses axon sprouting by somatostatin interneurons in a mouse model of temporal lobe epilepsy. Epilepsia, 52(11), 2057–2064. 10.1111/j.1528-1167.2011.03253.x [PubMed: 21883182]

Butler CR, Boychuk JA, Smith BN (2015) Effects of rapamycin treatment on neurogenesis and synaptic reorganization in the dentate gyrus after controlled cortical impact injury in mice. Frontiers in Systems Neuroscience, 9, 163. 10.3389/fnsys.2015.00163 [PubMed: 26640431]

Carson RP, Fu C, Winzenburger P, Ess KC (2013) Deletion of Rictor in neural progenitor cells reveals contributions of mTORC2 signaling to tuberous sclerosis complex. Human Molecular Genetics, 22(1), 140–152. 10.1093/hmg/dds414 [PubMed: 23049074]

Castle MJ, Gershenson ZT, Giles AR, Holzbaur EL, Wolfe JH (2014) Adeno-associated virus serotypes 1,8, and 9 share conserved mechanisms for anterograde and retrograde axonal transport. Human Gene Therapy, 25(8), 705–720. 10.1089/hum.2013.189 [PubMed: 24694006]

Chen CJ, Sgritta M, Mays J, Zhou H, Lucero R, Park J, Wang IC, Park JH, Kaipparettu BA, Stoica L, Jafar-Nejad P, Rigo F, Chin J, Noebels JL, Costa-Mattioli M (2019) Therapeutic inhibition of mTORC2 rescues the behavioral and neurophysiological abnormalities associated with Pten-deficiency. Nature Medicine, 25, 1684–1690. 10.1038/s41591-019-0608-y

Chen LL, Wu ML, Zhu F, Kai JJ, Dong JY, Wu XM, Zeng LH (2016) Neural progenitor cells Rptor ablation impairs development but benefits to seizure-induced behavioral abnormalities. CNS Neuro Ther, 22, 1000–1008. 10.1111/cns.12607

Chu Y, Fioravante D, Leitges M, Regehr WG (2014) Calcium-dependent PKC isoforms have specialized roles in short-term synaptic plasticity. Neuron, 82(4), 859–871. 10.1016/j.neuron.2014.04.003 [PubMed: 24794094]

Citraro R, Leo A, Constanti A, Russo E, De Sarro G (2016) mTOR pathway inhibition as a new therapeutic strategy in epilepsy and epileptogenesis. Pharmacological Research, 107, 333–343. 10.1016/j.phrs.2016.03.039 [PubMed: 27049136]

Cloëtta D, Thomanetz V, Baranek C, Lustenberger RM, Lin S, Oliveri F, Atanasoski S, Rüegg MA (2013) Inactivation of mTORC1 in the developing brain causes microcephaly and affects gliogenesis. The Journal of Neuroscience, 33(18), 7799–7810. 10.1523/jneurosci.3294-12.2013 [PubMed: 23637172]

Danzer SC, He X, Loepke AW, McNamara JO (2010) Structural plasticity of dentate granule cell mossy fibers during the development of limbic epilepsy. Hippocampus, 20(1), 113–124. 10.1002/hipo.20589 [PubMed: 19294647]

Fujita Y, Sasaki T, Fukui K, Kotani H, Kimura T, Hata Y, Südhof TC, Scheller RH, Takai Y (1996) Phosphorylation of Munc-18/n-Sec1/rbSec1 by Protein Kinase C: Its implication in regulating the interaction of Munc-18ITS /n-Sec1/rbSec1 with syntaxin. Journal of Biological Chemistry, 271(13), 7265–7268. 10.1074/jbc.271.13.7265 [PubMed: 8631738]

Gericke B, Brandt C, Theilmann W, Welzel L, Schidlitzki A, Twele F, Kaczmarek E, Anjum M, Hillmann P, Löscher W (2020) Selective inhibition of mTORC1/2 or PI3K/mTORC1/2 signaling does not prevent or modify epilepsy in the intrahippocampal kainate mouse model. Neuropharmacology, 162, 107817. 10.1016/j.neuropharm.2019.107817 [PubMed: 31654704]

Godale CM, Danzer SC (2018) Signaling pathways and cellular mechanisms regulating mossy fiber sprouting in the development of epilepsy. Frontiers in Neurology, 9. 10.3389/fneur.2018.00298

Guo D, Zeng L, Brody DL, Wong M (2013) Rapamycin attenuates the development of posttraumatic epilepsy in a mouse model of traumatic brain injury. PloS One, 8(5), e64078–e64078. 10.1371/journal.pone.0064078 [PubMed: 23691153]

Heinemann U, Beck H, Dreier JP, Ficker E, Stabel J, Zhang CL (1992) The dentate gyrus as a regulated gate for the propagation of epileptiform activity. Epilepsy Research. Supplement, 7, 273–280. [PubMed: 1334666]

Hernandez D, Torres CA, Setlik W, Cebrián C, Mosharov EV, Tang G, Cheng HC, Kholodilov N, Yarygina O, Burke RE, Gershon M, Sulzer D (2012) Regulation of presynaptic neurotransmission by macroautophagy. Neuron, 74(2), 277–284. 10.1016/j.neuron.2012.02.020 [PubMed: 22542182]

Hester MS, Danzer SC (2013) Accumulation of abnormal adult-generated hippocampal granule cells predicts seizure frequency and severity. The Journal of Neuroscience, 33(21), 8926–8936. 10.1523/jneurosci.5161-12.2013 [PubMed: 23699504]

Hester MS, Hosford BE, Santos VR, Singh SP, Rolle IJ, LaSarge CL, Liska JP, Garcia-Cairasco N, Danzer SC (2016) Impact of rapamycin on status epilepticus induced hippocampal pathology and weight gain. Experimental Neurology, 280, 1–12. 10.1016/j.expneurol.2016.03.015 [PubMed: 26995324]

Hofacer RD, Deng M, Ward CG, Joseph B, Hughes EA, Jiang C, Danzer SC, Loepke AW (2013) Cell age–specific vulnerability of neurons to anesthetic toxicity. Annals of Neurology, 73(6), 695–704. 10.1002/ana.23892 [PubMed: 23526697]

Jiang Y, Tong D, Hofacer RD, Loepke AW, Lian Q, Danzer SC (2016) Long-term fate mapping to assess the impact of postnatal isoflurane exposure on hippocampal progenitor cell productivity. Anesthesiology, 125(6), 1159–1170. 10.1097/ALN.0000000000001358 [PubMed: 27655218]

Ka M, Smith AL, Kim WY (2017) mTOR controls genesis and autophagy of GABAergic interneurons during brain development. Autophagy, 13(8), 1348–1363. 10.1080/15548627.2017.1327927 [PubMed: 28598226]

Karalis V, Bateup HS (2021) Current approaches and future directions for the treatment of mTORopathies. Dev Neurosci, 43, 143–158. 10.1159/000515672 [PubMed: 33910214]

Kim DH, Sarbassov DD, Ali SM, King JE, Latek RR, Erdjument-Bromage H, Tempst P, Sabatini DM (2002). TOR interacts with raptor to form a nutrient-sensitive complex that signals to the cell growth machinery. Cell, 110(2), 163–175. 10.1016/S0092-8674(02)00808-5 [PubMed: 12150925]

Koyama R, Ikegaya Y (2018) The molecular and cellular mechanisms of axon guidance in mossy fiber sprouting. Frontiers in Neurology, 9. 10.3389/fneur.2018.00382

Kron MM, Zhang H, Parent JM (2010) The developmental stage of dentate granule cells dictates their contribution to seizure-induced plasticity. The Journal of Neuroscience, 30(6), 2051–2059. 10.1523/jneurosci.5655-09.2010 [PubMed: 20147533]

Krook-Magnuson E, Armstrong C, Oijala M, Soltesz I (2013) On-demand optogenetic control of spontaneous seizures in temporal lobe epilepsy. Nature Communications, 4, 1376. 10.1038/ncomms2376

Krook-Magnuson E, Armstrong C, Bui A, Lew S, Oijala M, Soltesz I (2015) In vivo evaluation of the dentate gate theory in epilepsy. The Journal of Physiology, 593(10), 2379–2388. 10.1113/JP270056 [PubMed: 25752305]

LaSarge CL, Pun RYK, Gu Z, Riccetti MR, Namboodiri DV, Tiwari D, Gross C, Danzer SC (2021) mTOR-driven neural circuit changes initiate an epileptogenic cascade. Progress in Neurobiology, 200, 101974. 10.1016/j.pneurobio.2020.101974 [PubMed: 33309800]

Löscher W (2020) The holy grail of epilepsy prevention: Preclinical approaches to antiepileptogenic treatments. Neuropharmacology, 167, 107605. 10.1016/j.neuropharm.2019.04.011 [PubMed: 30980836]

Macias M, Blazejczyk M, Kazmierska P, Caban B, Skalecka A, Tarkowski B, Rodo A, Konopacki J, Jaworski J (2013) Spatiotemporal characterization of mTOR kinase activity following kainic acid induced status epilepticus and analysis of rat brain response to chronic rapamycin treatment. PloS One, 8(5), e64455–e64455. 10.1371/journal.pone.0064455 [PubMed: 23724051]

Madisen L, Zwingman TA, Sunkin SM, Oh SW, Zariwala HA, Gu H, Ng LL, Palmiter RD, Hawrylycz MJ, Jones AR, Lein ES, Zeng H (2010) A robust and high-throughput Cre reporting and characterization system for the whole mouse brain. Nat Neurosci. 13(1):133–40. [PubMed: 20023653]

Magee JA, Ikenoue T, Nakada D, Lee JY, Guan KL, Morrison SJ (2012) Temporal changes in PTEN and mTORC2 regulation of hematopoietic stem cell self-renewal and leukemia suppression. Cell Stem Cell, 11(3), 415–428. 10.1016/j.stem.2012.05.026 [PubMed: 22958933]

Malik R, Pai ELL, Rubin AN, Stafford AM, Angara K, Minasi P, Rubenstein JL, Sohal VS, Vogt D (2019) Tsc1 represses parvalbumin expression and fast-spiking properties in somatostatin lineage cortical interneurons. Nature Communications, 10(1), 4994. 10.1038/s41467-019-12962-4

McCabe MP, Cullen ER, Barrows CM, Shore AN, Tooke KI, Laprade KA, Stafford JM, Weston MC (2020) Genetic inactivation of mTORC1 or mTORC2 in neurons reveals distinct functions in glutamatergic synaptic transmission. ELife, 9, e51440. 10.7554/eLife.51440 [PubMed: 32125271]

Murphy BL, Hofacer RD, Faulkner CN, Loepke AW, Danzer SC (2012) Abnormalities of granule cell dendritic structure are a prominent feature of the intrahippocampal kainic acid model of epilepsy despite reduced postinjury neurogenesis. Epilepsia, 53(5), 908–921. 10.1111/j.1528-1167.2012.03463.x [PubMed: 22533643]

Nguyen LH, Bordey A (2021) Convergent and divergent mechanisms of epileptogenesis in mTORopathies. In Frontiers in Neuroanatomy (Vol. 15). 10.3389/fnana.2021.715363

Okamoto OK, Janjoppi L, Bonone FM, Pansani AP, da Silva AV, Scorza FA, Cavalheiro EA (2010) Whole transcriptome analysis of the hippocampus: toward a molecular portrait of epileptogenesis. BMC Genomics, 11, 230. 10.1186/1471-2164-11-230 [PubMed: 20377889]

Peng Z, Houser CR (2005) Temporal patterns of fos expression in the dentate gyrus after spontaneous seizures in a mouse model of temporal lobe epilepsy. The Journal of Neuroscience, 25(31), 7210–7220. 10.1523/jneurosci.0838-05.2005 [PubMed: 16079403]

Peterson TR, Sengupta SS, Harris TE, Carmack AE, Kang SA, Balderas E, Guertin DA, Madden KL, Carpenter AE, Finck BN, Sabatini DM (2011) mTOR complex 1 regulates lipin 1 localization to control the SREBP pathway. Cell, 146(3), 408–420. 10.1016/j.cell.2011.06.034 [PubMed: 21816276]

Pun RYK, Rolle IJ, LaSarge CL, Hosford BE, Rosen JM, Uhl JD, Schmeltzer SN, Faulkner C, Bronson SL, Murphy BL, Richards DA, Holland KD, Danzer SC (2012) Excessive activation of mTOR in postnatally generated granule cells is sufficient to cause epilepsy. Neuron, 75(6), 1022–1034. 10.1016/j.neuron.2012.08.002 [PubMed: 22998871]

Racine RJ (1972) Modification of seizure activity by electrical stimulation: II. Motor seizure. Electroencephalography and Clinical Neurophysiology, 32(3), 281–294. 10.1016/0013-4694(72)90177-0 [PubMed: 4110397]

Sarbassov DD, Ali SM, Kim DH, Guertin DA, Latek RR, Erdjument-Bromage H, Tempst P, Sabatini DM (2004) Rictor, a novel binding partner of mTOR, defines a rapamycin-insensitive and raptor-independent pathway that regulates the cytoskeleton. Current Biology, 14(14), 1296–1302. 10.1016/j.cub.2004.06.054 [PubMed: 15268862]

Sarbassov DD, Ali SM, Sabatini DM (2005) Growing roles for the mTOR pathway. Current Opinion in Cell Biology, 17(6), 596–603. 10.1016/j.ceb.2005.09.009 [PubMed: 16226444]

Sengupta S, Peterson TR, Laplante M, Oh S, Sabatini DM (2010) mTORC1 controls fasting-induced ketogenesis and its modulation by ageing. Nature, 468(7327), 1100–1104. 10.1038/nature09584 [PubMed: 21179166]

Talos DM, Jacobs LM, Gourmaud S, Coto CA, Sun H, Lim KC, Lucas TH, Davis KA, Martinez-Lage M, Jensen FE (2018) Mechanistic target of rapamycin complex 1 and 2 in human temporal lobe epilepsy. Annals of Neurology, 83(2), 311–327. 10.1002/ana.25149 [PubMed: 29331082]

Tang F, Wu Q, Ikenoue T, Guan KL, Liu Y, Zheng P (2012b) A critical role for Rictor in T lymphopoiesis. Journal of Immunology, 189(4), 1850–1857. 10.4049/jimmunol.1201057

Tang H, Long H, Zeng C, Li Y, Bi F, Wang J, Qian H, Xiao B (2012a) Rapamycin suppresses the recurrent excitatory circuits of dentate gyrus in a mouse model of temporal lobe epilepsy. Biochemical and Biophysical Research Communications, 420(1), 199–204. 10.1016/j.bbrc.2012.02.143 [PubMed: 22414694]

Tang SJ, Reis G, Kang H, Gingras AC, Sonenberg N, Schuman EM (2002) A rapamycin-sensitive signaling pathway contributes to long-term synaptic plasticity in the hippocampus. Proceedings of the National Academy of Sciences, 99(1), 467–472. 10.1073/pnas.012605299

Theilmann W, Gericke B, Schidlitzki A, Muneeb Anjum SM, Borsdorf S, Harries T, Roberds SL, Aguiar DJ, Brunner D, Leiser SC, Song D, Fabbro D, Hillmann P, Wymann MP, Löscher W (2020) Novel brain permeant mTORC1/2 inhibitors are as efficacious as rapamycin or everolimus in mouse models of acquired partial epilepsy and tuberous sclerosis complex. Neuropharmacology, 180 10.1016/j.neuropharm.2020.108297.

Thomanetz V, Angliker N, Cloëtta D, Lustenberger RM, Schweighauser M, Oliveri F, Suzuki N, Rüegg MA (2013) Ablation of the mTORC2 component rictor in brain or Purkinje cells affects size and neuron morphology. The Journal of Cell Biology, 201(2), 293–308. 10.1083/jcb.201205030 [PubMed: 23569215]

Vezzani A, Balosso S, Ravizza T (2019) Neuroinflammatory pathways as treatment targets and biomarkers in epilepsy. Nature Reviews Neurology, 15(8), 459–472. 10.1038/s41582-019-0217-x [PubMed: 31263255]

Walter C, Murphy BL, Pun RYK, Spieles-Engemann AL, Danzer SC (2007) Pilocarpine-induced seizures cause selective time-dependent changes to adult-generated hippocampal dentate granule cells. The Journal of Neuroscience, 27(28), 7541–7552. 10.1523/jneurosci.0431-07.2007 [PubMed: 17626215]

Wang X, Zhang C, Szábo G, Sun QQ, (2013) Distribution of CaMKIIα expression in the brain in vivo, studied by CaMKIIα-GFP mice. Brain Research, 1518, 9–25. 10.1016/j.brainres.2013.04.042 [PubMed: 23632380]

Wang Y, Barbaro MF, Baraban SC (2006) A role for the mTOR pathway in surface expression of AMPA receptors. Neuroscience Letters, 401(1), 35–39. 10.1016/j.neulet.2006.03.011 [PubMed: 16677760]

Weston MC, Chen H, Swann JW (2012) Multiple roles for mammalian target of rapamycin signaling in both glutamatergic and GABAergic synaptic transmission. The Journal of Neuroscience, 32(33), 11441–11452. 10.1523/jneurosci.1283-12.2012 [PubMed: 22895726]

Williams MR, DeSpenza T, Li M, Gulledge AT, Luikart BW (2015) Hyperactivity of newborn Pten knock-out neurons results from increased excitatory synaptic drive. The Journal of Neuroscience, 35(3), 943–959. 10.1523/jneurosci.3144-14.2015 [PubMed: 25609613]

Wulsin A, Herman J, Danzer S (2016) RU486 mitigates hippocampal pathology following status epilepticus. Frontiers in Neurology, 7. 10.3389/fneur.2016.00214

Wulsin A, Kraus K, Gaitonde K, Suru V, Arafa S, Packard BA, Herman JP, Danzer SC (2021) The glucocorticoid receptor specific modulator CORT108297 reduces brain pathology following status epilepticus. Experimental Neurology, 341, 113703. 10.1016/j.expneurol.2021.113703 [PubMed: 33745919]

Xiong Q, Oviedo HV, Trotman LC, Zador AM (2012) PTEN regulation of local and long-range connections in mouse auditory cortex. The Journal of Neuroscience, 32(5), 1643–1652. 10.1523/jneurosci.4480-11.2012 [PubMed: 22302806]

Yamawaki R, Thind K, Buckmaster PS (2015) Blockade of excitatory synaptogenesis with proximal dendrites of dentate granule cells following rapamycin treatment in a mouse model of temporal lobe epilepsy. The Journal of Comparative Neurology, 523(2), 281–297. 10.1002/cne.23681 [PubMed: 25234294]

Zeng LH, Rensing NR, Wong M (2009) The mammalian target of rapamycin signaling pathway mediates epileptogenesis in a model of temporal lobe epilepsy. The Journal of Neuroscience, 29(21), 6964–6972. 10.1523/jneurosci.0066-09.2009 [PubMed: 19474323]

Zhao XF, Liao Y, Alam MM, Mathur R, Feustel P, Mazurkiewicz JE, Adamo MA, Zhu XC, Huang Y (2020) Microglial mTOR is neuronal protective and antiepileptogenic in the pilocarpine model of temporal lobe epilepsy. The Journal of Neuroscience, 40(40), 7593–7608. 10.1523/jneurosci.2754-19.2020 [PubMed: 32868461]

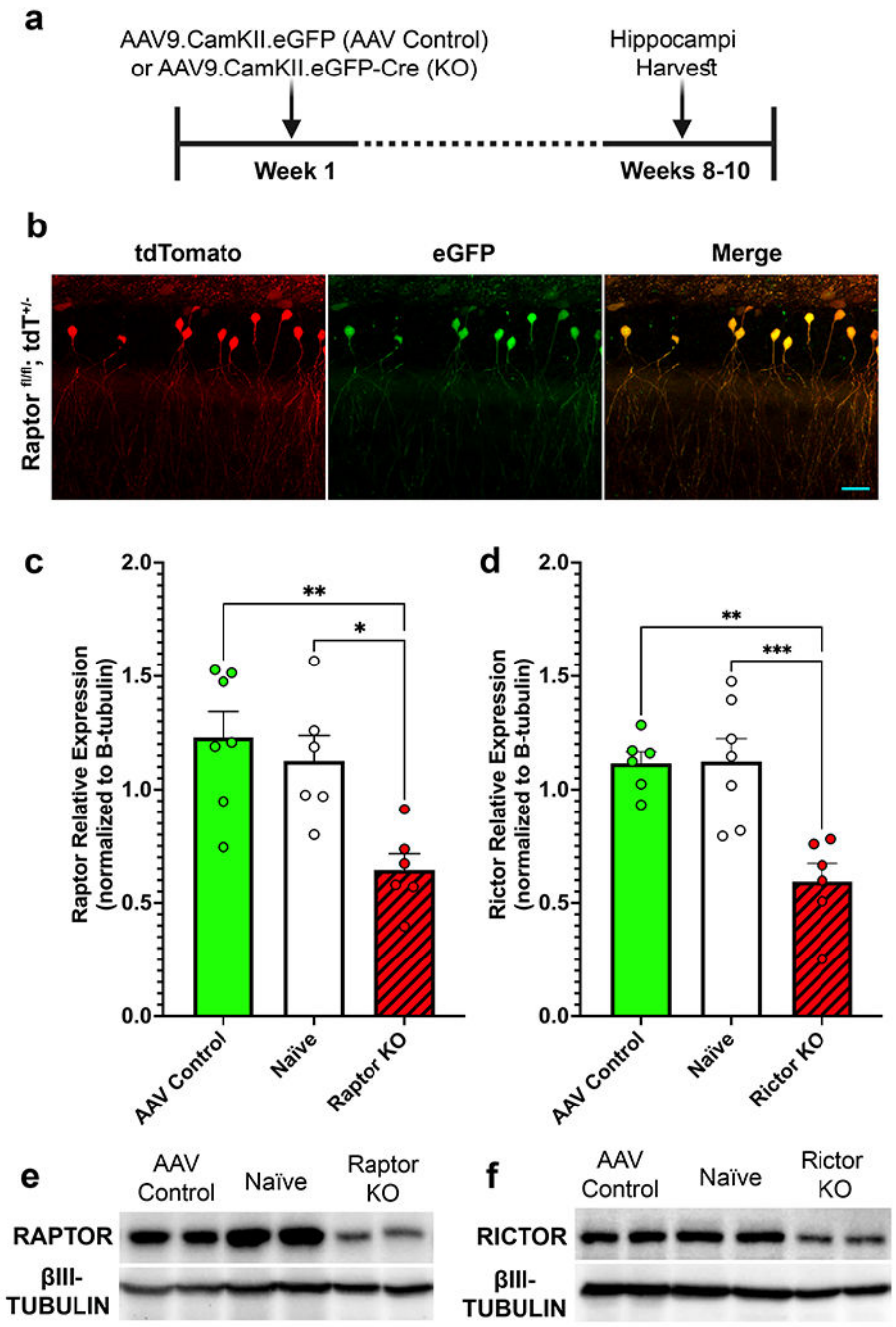

Fig. 1.

(a): Experimental timeline for western blot experiments. Double transgenic mice were injected with either a control virus (AAV control; AAV9.CamKII.eGFP), a cre-expressing virus (KO; AAV9.CamKII.eGFP-Cre) or underwent no treatments (naïve). (b): Raptor$^{fl/fl}$;tdTomato$^{+/-}$ mice injected with AAV9.CamKII.eGFP-Cre show colocalization between tdTomato and eGFP in dentate granule cells. Scale bar = 25 μm. (c): eGFP-Cre significantly decreased Raptor protein expression in the hippocampus relative to Raptor AAV and naïve controls. (d): eGFP-Cre significantly decreased Rictor protein expression in

the hippocampus relative to Rictor AAV and naïve controls. (e, f): Example western blots for Raptor and Rictor experiments, respectively.

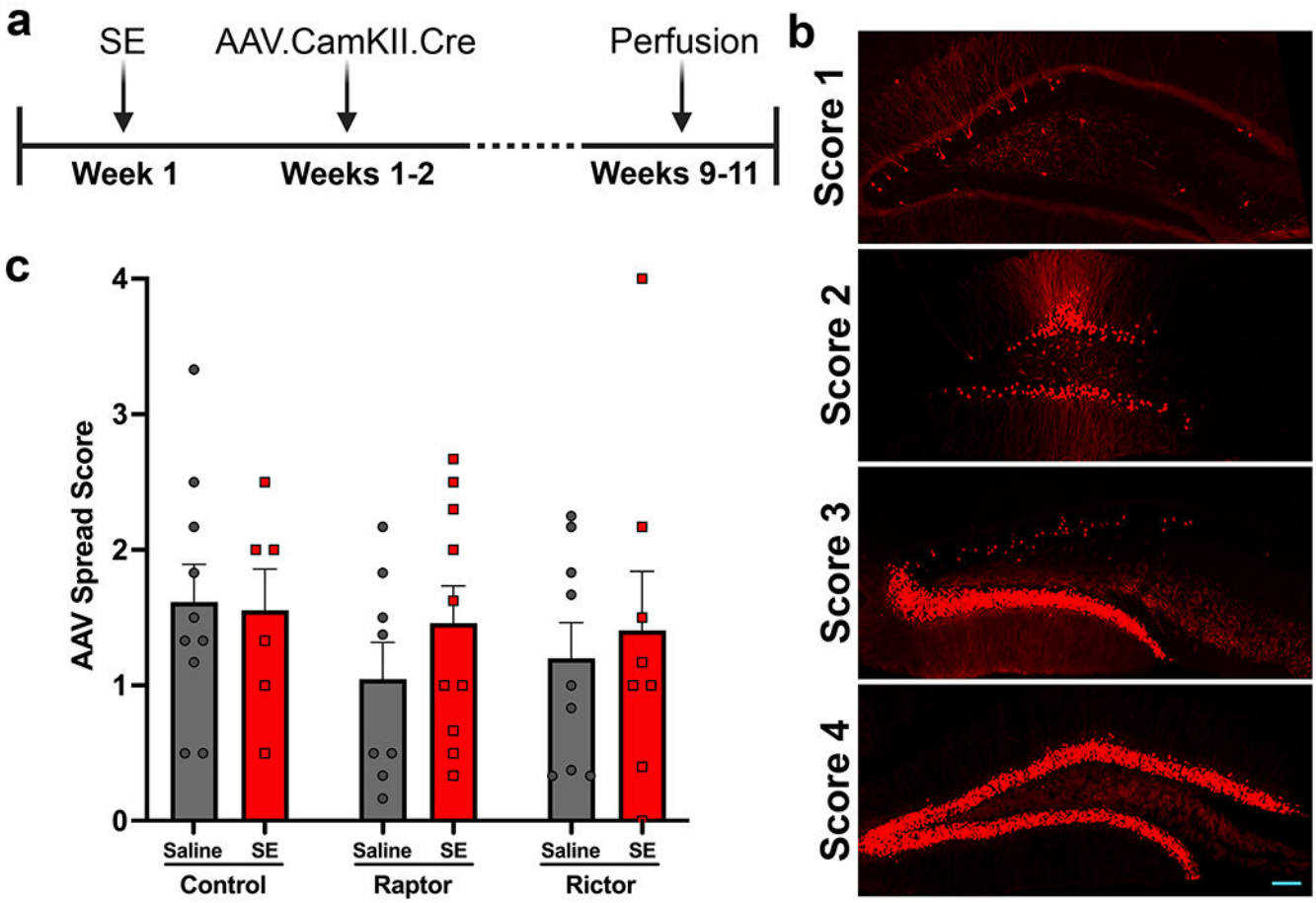

Fig. 2.

(a): Experimental timeline for Raptor/Rictor deletion after status epilepticus (SE). **(b):** To assess viral spread, tdTomato expression in the dentate gyrus of each animal was scored using a semiquantitative 0-4 scale. Scale bar = 100 μm. **(c):** Mean scores ± SEM for the percentage of virally infected (tdTomato labeled) dentate granule cells in each mouse.

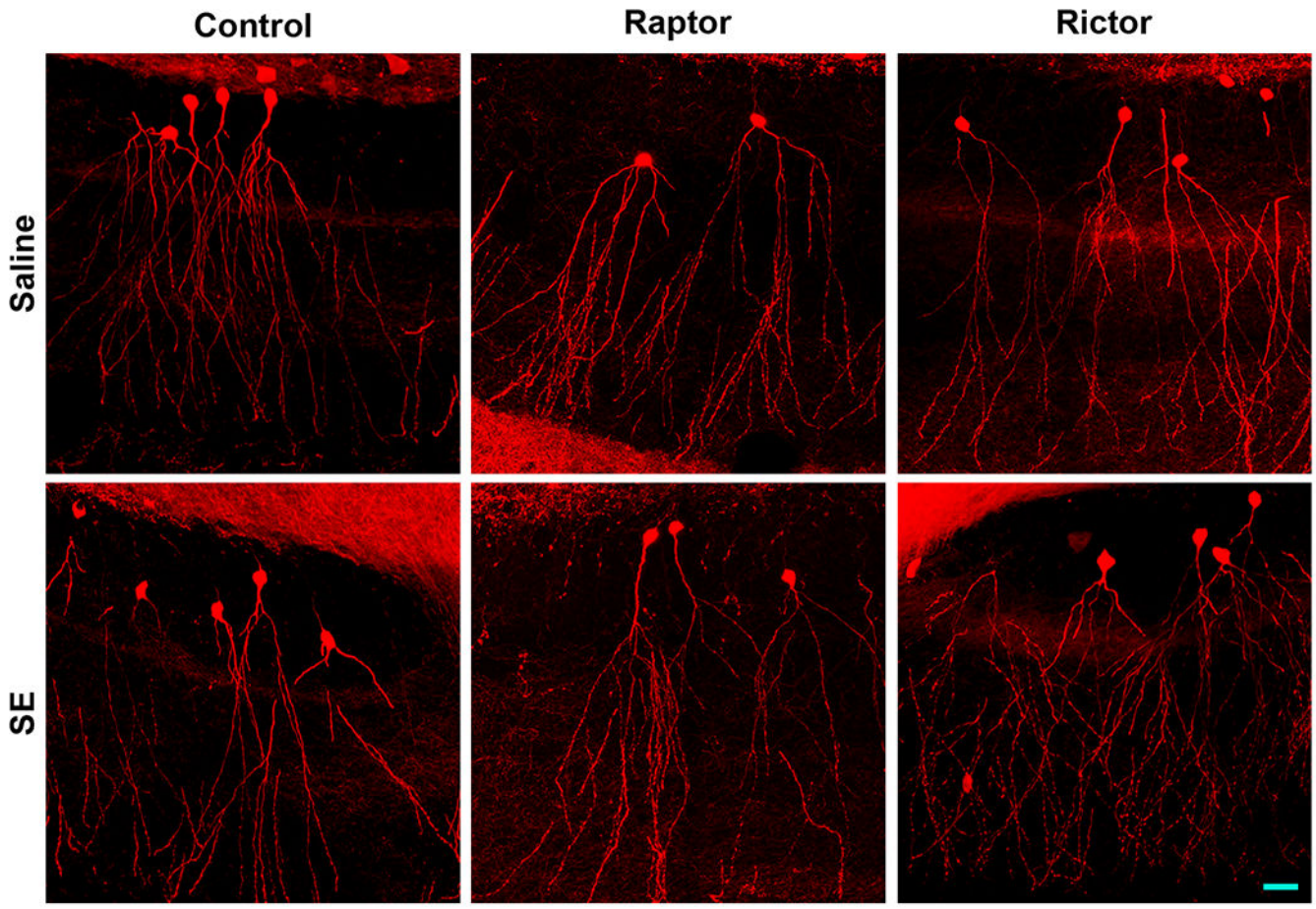

Fig. 3.

Confocal maximum projections of tdTomato-labeled granule cells from all 6 groups. No gross structural abnormalities or evidence of degenerative changes were observed. Scale bar = 20 μm.

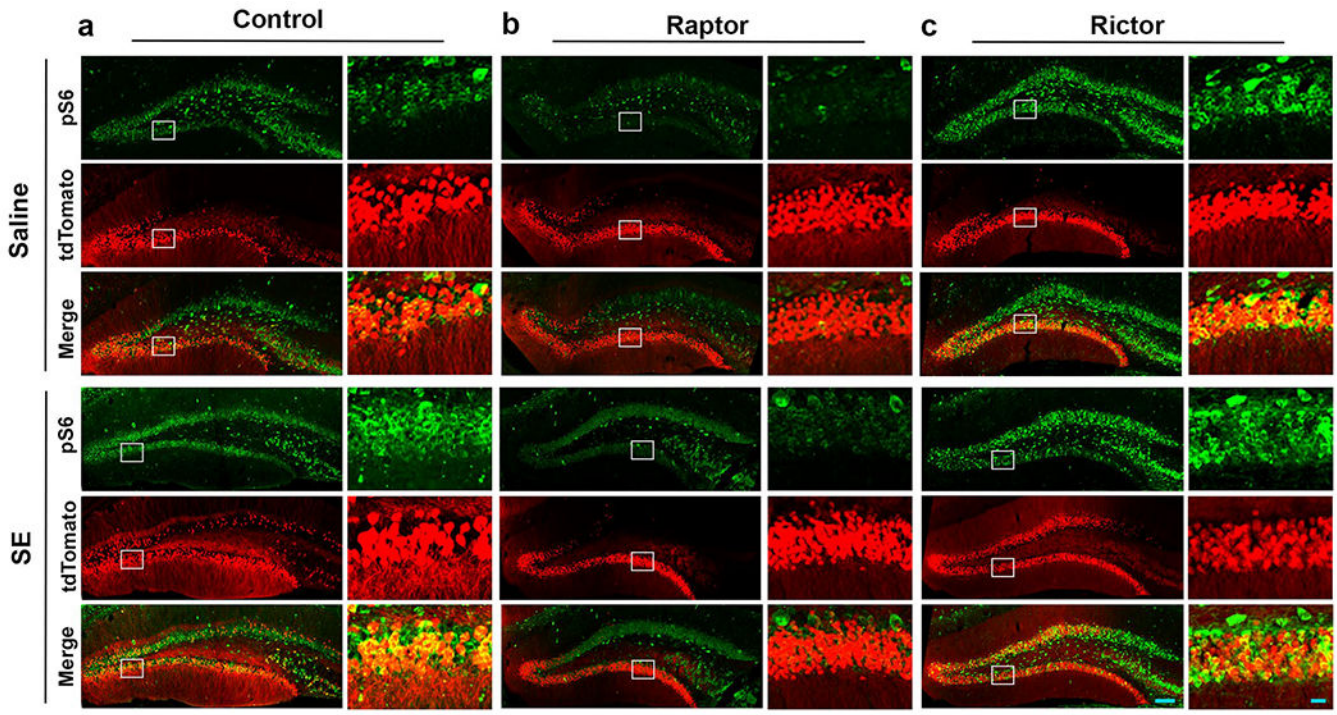

Fig. 4.

(a-c): Confocal maximum projections of tdTomato-labeled (red) dentate granule cells immunostained for pS6 (green). Images show the dentate gyrus, while boxed regions are expanded to the left for each set. In control (a) and Rictor KO animals, colocalization between tdTomato and pS6 is clear in the expansions. In Raptor$^{fl/fl}$ mice, however, tdTomato-labeled cells were only rarely immunoreactive for pS6. Findings support the efficacy of Raptor deletion at the single cell level. Occasional double positive cells in these animals likely reflect incomplete recombination events. Scale bars = 100 μm and 20 μm (inset).

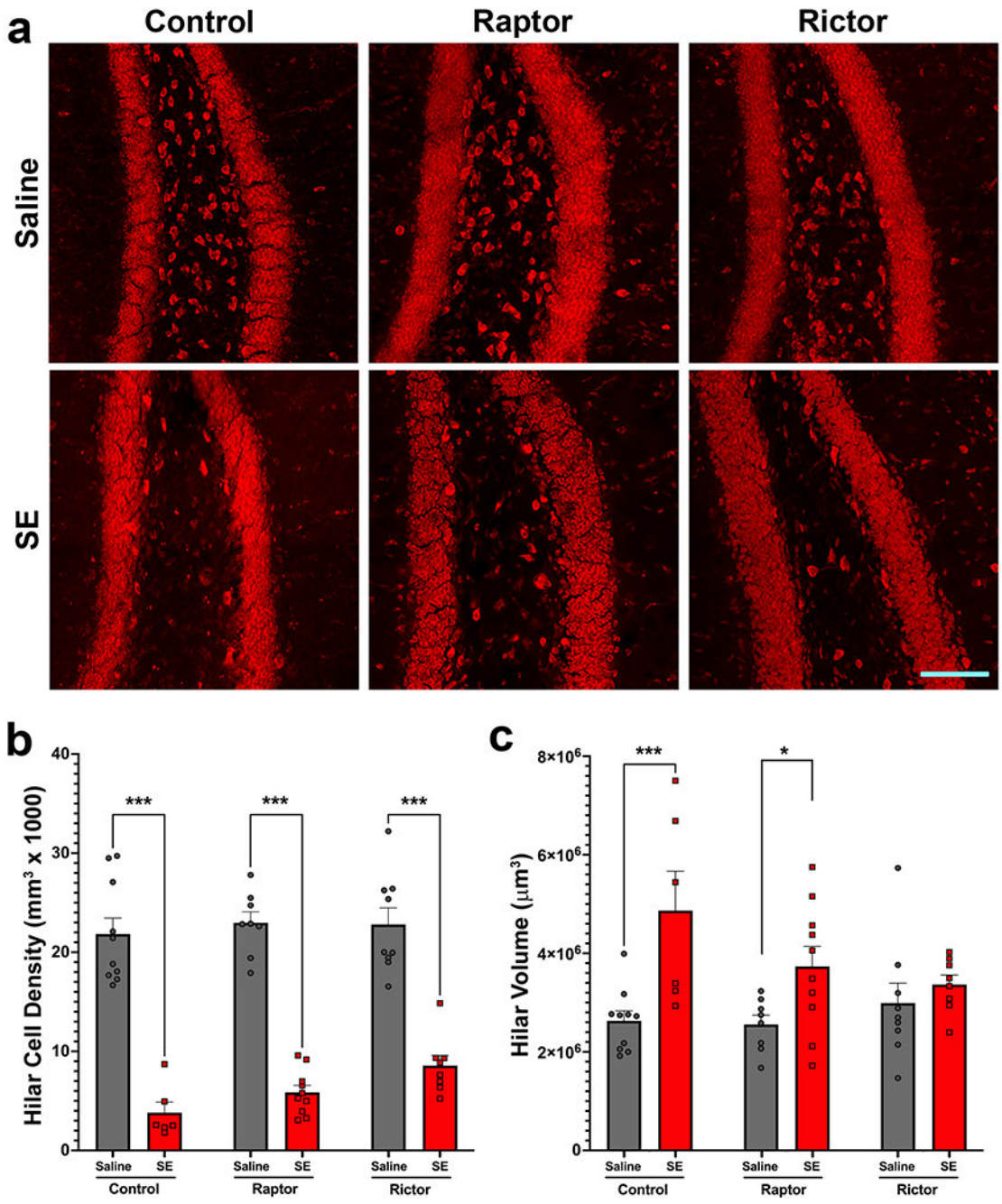

Fig. 5.

(a) Confocal maximum projections of Nissl staining in the dentate hilus. Hilar cell loss is clear among animals that underwent SE. Scale bar = 100 µm. (b) Hilar cell density was significantly reduced in SE animals relative to saline animals in all cohorts. No effect of Raptor or Rictor deletion on cell loss was evident. **(c)** SE produced a significant increase in hilar volume within wildtype and Raptor groups. Although increases in volume in Raptor and Rictor KOs was less than that observed in controls, no significant effects of genotype were found. ***, $p<0.001$. *, $p<0.05$.

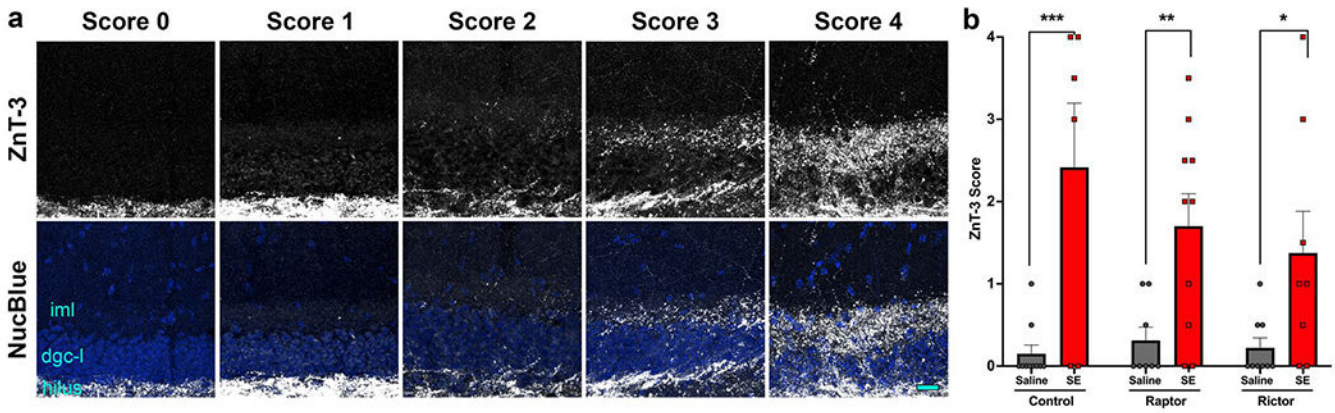

Fig. 6.

(a): Brain sections immunostained with ZnT-3 were screened to identify mossy fiber sprouting, evident as ZnT-3 immunoreactive puncta (shown in white) in the dentate inner molecular layer (iml). Each animal was scored using a semi-quantitative 0-4 scale (0= no sprouting, 4= robust sprouting). Scale bar = 20 μm. (b) SE significantly increased mossy fiber sprouting in all genotypes, however, no differences among genotypes were found. ***, $p<0.001$. **, $p<0.01$. *, $p<0.05$.

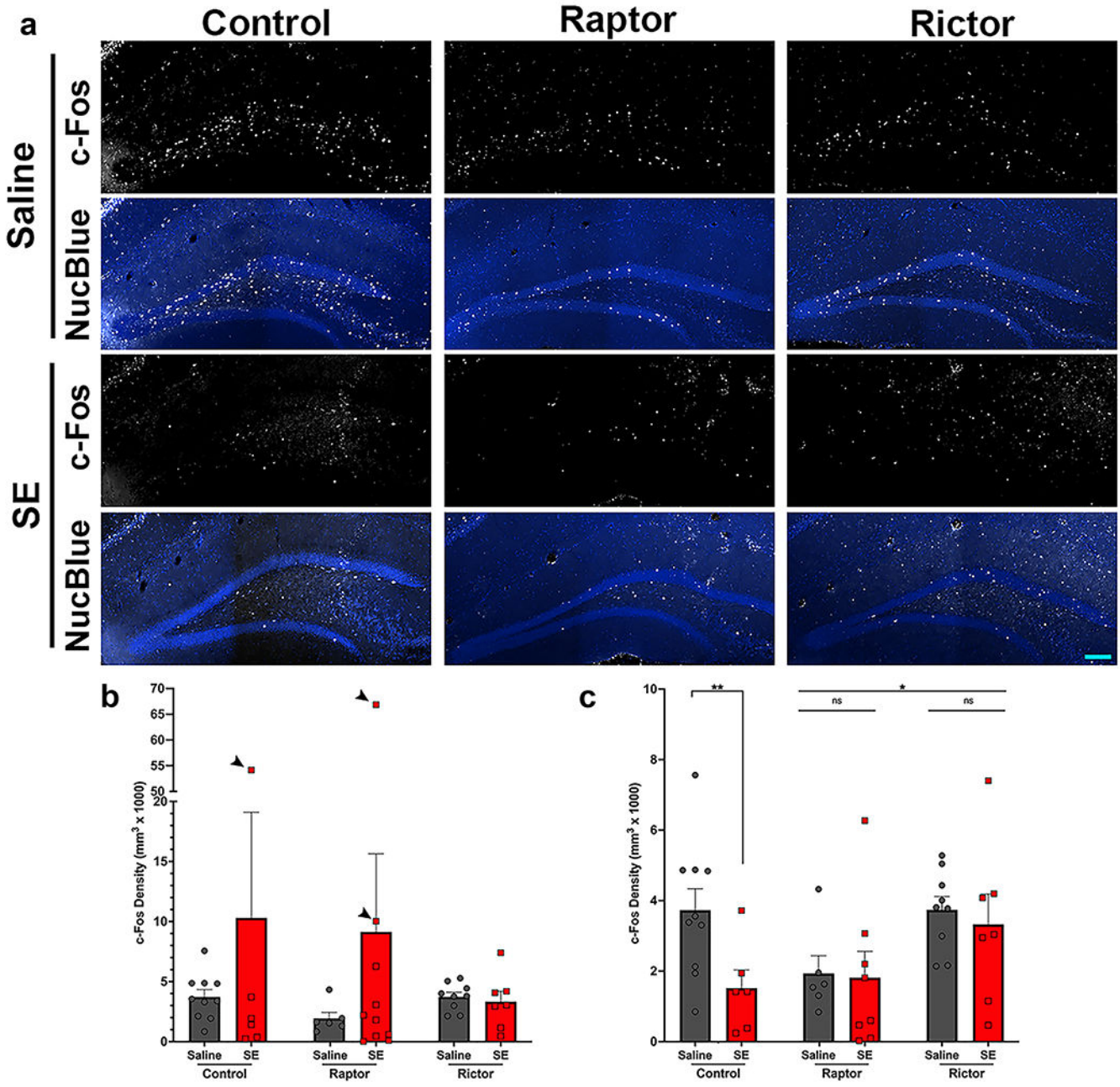

Fig. 7.

(a) c-Fos immunoreactivity (white) and NucBlue staining (blue) in the dentate gyrus. Scale bar = 100 μm. **(b)** Graph shows the density of c-Fos immunoreactive cells in the dentate. Groups did not differ significantly. Arrowheads indicate outliers. **(c)** Replotting of the data in b after removing 3 outliers (likely animals that experienced seizures shortly before sacrifice). With outliers excluded, SE was found to reduce c-Fos density within controls and density in the Raptor groups was reduced compared to Rictor groups. *, $p<0.05$. **, $p<0.01$. ns, not significant.

Table 1.

Animal genotype, treatments, and sex distribution for each group.

Group Name	Genotype	Treatment	Time from treatment to AAV injection (days)	Virus*	Males (N)	Females (N)	Survival time after AAV (wks)
No-SE, Wildtype	$tdTomato^{+/-}$	Saline	8.7±0.4 [7-10]	AAV9-Cre	5	5	8.9±0.2 [7.7-9.3]
SE Wildtype	$tdTomato^{+/-}$	Pilocarpine SE	6.2±0.9 [4-10]	AAV9-Cre	5	1	9.2±0.4 [8-10]
No-SE, Raptor KO	$Raptor^{fl/fl}$, $tdTomato^{+/-}$	Saline	8.1±0.4 [7-10]	AAV9-Cre	3	5	8.1±0.1 [7.7-9]
SE + Raptor KO	$Raptor^{fl/fl}$, $tdTomato^{+/-}$	Pilocarpine SE	7.8±0.6 [5-11]	AAV9-Cre	8	2	8.4±0.2 [7.6-9.1]
No-SE, Rictor KO	$Rictor^{fl/fl}$, $tdTomato^{+/-}$	Saline	11.0±1.0 [7-14]	AAV9-Cre	3	6	8.1±0.2 [7.6-8.7]
SE + Rictor KO	$Rictor^{fl/fl}$, $tdTomato^{+/-}$	Pilocarpine SE	8.3±0.5 [7-10]	AAV9-Cre	3	5	8.6±0.4 [7.1-10]

*All animals were injected with a cocktail of AAV9-Cre and AAV9-eGFP virus (the latter as part of another study). Times are means±SEM [range].

Table 2.

Percentage of animals in each group for which tdT+ expression in the dentate gyrus, CA3, CA1, thalamus, or cortex was present.

Animal Group	Dentate Gyrus	CA3	CA1	Thalamus	Cortex
No-SE, Wildtype	100%	63.33%	46.67%	21.67%	0%
SE Wildtype	100%	55.56%	19.44%	8.33%	0%
No-SE, Raptor KO	100%	31.25%	25%	14.58%	2.08%
SE + Raptor KO	100%	31.82%	21.21%	10.61%	0%
No-SE, Rictor KO	100%	35.19%	50%	3.75%	0%
SE + Rictor KO	100%	54.17%	37.5%	16.67%	0%